This is the submitted version of Lindsay, J.B., Cockburn, J.M.H., and Russell, H.A.J., 2015. An integral image approach to performing multi-scale topographic position analysis, *Geomorphology*, 245(15), 51-61, which has been published in final form at doi:10.1016/j.geomorph.2015.05.025. This article may be used for non-commercial purposes only.

An integral image approach to performing multi-scale topographic position analysis

J.B. Lindsay[a,*], J.M.H. Cockburn[a], and H.A.J. Russell[b]

[a] Department of Geography, University of Guelph, 50 Stone Road East, Guelph, N1G 2W1, Canada

[b] Geological Survey of Canada, Natural Resources Canada, 601 Booth St., Ottawa, K1A 0E8, Canada

*Corresponding author. Tel: +1 519 824-4120 ext. 56074

E-mail address: jlindsay@uoguelph.ca (J.B. Lindsay)

Abstract

Digital elevation model (DEM) derived measures of terrain ruggedness and relative topographic position are useful parameters for automated landform classification and are widely applied in soils, vegetation, and habitat mapping. These elevation residual attributes are inherently scale dependent because they are defined in the context of a local neighborhood. Several previous studies have focused on assessing the multi-scale properties of elevation residuals based on varying roving window sizes, DEM grid resolution resampling, and hierarchical object-based methods. The computationally intensive nature of large-window DEM filtering has previously prevented the application of the varying roving window size approach from being applied to study the scaling properties of the terrain ruggedness and topographic position at broader regional scales.

This paper explores the use of an integral image based approach to measuring the common relative topographic position metric deviation from mean elevation (*DEV*). The approach was applied to a large DEM of an extensive and heterogeneous region in eastern North America. Compared with traditional image filtering techniques, the integral image approach was extremely efficient for calculating *DEV*, enabling a fine-resolution multi-scale analysis of elevation residuals. A method is described to allow for the measurement of *DEV* at optimal scales for each grid cell within wide spatial scale ranges. A novel technique is also developed for visualizing the scaling characteristics of topographic position using color composite imagery.

Highlights

- Measures of relative topographic position are widely applied in geomorphology.
- Traditional methods used to estimate topographic position are highly inefficient.
- Integral images are used here to measuring indices of topographic position.
- The approach's efficiency enables detailed multi-scaled topographic analysis.

Keywords

Geomorphometry; Digital elevation models; Scale; Topographic position; Ruggedness; Relief

1. Introduction

Topography is the general character of rough, complex, and irregular shaped surfaces. The concept of topography is most commonly applied to Earth's uneven surface (Huggett and Cheesman, 2002) and is the focus of research in geography and geology and their related fields of cartography, geodesy, geomorphology, and hydrology. This wide interest in studying Earth's topography is due to the partial control it has over the abundance and distribution of energy, water, nutrients, and sediments within landscapes (Lindsay and Rothwell, 2008). Topography is therefore strongly linked to environmental phenomena involving the distribution of flora and fauna and exerts substantial influence over spatial variability in climate (Böhner and Antonic, 2009).

Geomorphometry, also known as digital terrain analysis, is the field that is concerned with quantifying Earth's topography (Pike, 2000; Pike et al., 2008). Much of modern geomorphometry is focused on extracting information from DEMs. This process usually involves deriving topographic parameters from DEMs, including measures of local surface shape (e.g. slope gradient and curvature), orientation (i.e. slope aspect), and the related concepts of ruggedness and relative topographic position (Gallant and Wilson, 2000). It is this last class of attributes that is the focus of this paper. Ruggedness refers to the roughness of a surface while relative topographic position refers to how elevated a location is compared with its surroundings. Ruggedness and topographic position are useful for landform classification (Riley et al., 1999; Tagil and Jenness, 2008) and therefore are also commonly applied in soils, vegetation, and habitat mapping (Jenness, 2004). They are also properties affecting the exposure or sheltering of locations (Yokoyama et al., 2002; Lindsay and Rothwell, 2008).

Terrain shape attributes, such as slope and curvature, are theoretically defined for any point within the landscape. For a surface that can be expressed in mathematical form, it is possible to measure these shape parameters precisely for any

point on the surface. In practice, however, shape attributes are usually derived from a DEM using interpolated surfaces fitted to the elevations contained within the area of a 3×3 pixel roving window (Evans, 1984). This fact gives rise to a well-documented scale dependency (Chang and Tsai, 1991; Deng et al., 2007; Goodchild, 2011) that is typically viewed as a negative consequence of the way these terrain attributes are estimated. Ruggedness and topographic position by comparison are attributes that are inherently scale dependent because they can only be defined over an area. These attributes attempt to quantify the topographic character of a location within the broader context of its surroundings or local neighborhood. For example, a rocky outcrop situated on a valley bottom can be considered to be high in the landscape at shorter spatial scales but low-lying at a broader regional scale. The way that topographic position varies over a range of scales, i.e. the *scale signature* (Wood, 1996; Drăgut et al., 2011), can be viewed as valuable information for interpreting the structure of landscapes (Drăgut et al., 2011; De Reu et al., 2013).

Several approaches have been proposed for extracting this scale-variant topographic position information from DEMs including the use of a varying sized roving windows (e.g. Grohmann and Riccomini, 2009; De Reu et al., 2013), the resampling of DEM data to varying grid resolutions (e.g. Gallant and Dowling, 2003), and the use of a hierarchical object-based approach (e.g. Drăgut and Eisank, 2011). Scaling through resampling can result in generalization and loss of information due to smoothing (Deng et al., 2007; Drăgut and Eisank, 2011). The hierarchical object-based approach shows promise but adds the complexity and potential subjectivity involved in the object delineation process. Perhaps the most straightforward of the available techniques, the application of varying roving window sizes (i.e. raster spatial filtering) has the main disadvantage of being extremely computationally intensive (Deng and Wilson, 2008; Grohmann and Riccomini, 2009), which can make its application with large DEM datasets and regional-scale analyses impractical. This characteristic of the varying window size multi-scaling approach usually implies that relatively few window sizes can be used to sample the scale signature (Deng et al., 2007) and window sizes are often selected in an ad-hoc manner rather than optimally. These computational issues led Grohmann and Riccomini (2009) to conclude that the use of the roving window approach should be restricted to local scale analysis while resampling (i.e. what they refer to as a search window and interpolation method) can be used for broader spatial scales.

In the field of computer vision and graphics the problem of the computational inefficiency of large-window image filtering has been dealt with through the development of the integral image data transformation (Crow, 1984) and its more recent widespread application (Viola and Jones, 2001). The purpose of this study is to assess the use an integral-image based approach for performing multi-scale topographic position analyses on DEMs.

2. Background

2.1. Measures of ruggedness and topographic position

Gallant and Wilson (2000) provide a comprehensive review of existing indices for measuring ruggedness and topographic position, which they term *elevation residuals*. Elevation residuals are topographic indices derived from DEMs using spatial filtering techniques (i.e. a roving window of radius r is centered on each grid cell in the DEM) to quantify the spatial pattern of topographic position or ruggedness within the context of a surrounding area. Gallant and Wilson (2000) suggest defining neighborhoods with circular shaped windows, although square windows are more commonly used in practice. These terrain attributes are based on characteristics of the statistical frequency distribution of the elevations within neighborhoods defined by the roving window. All of the elevation residuals utilize location parameters (measures of central tendency) and/or scale parameters (measures of spread).

The two most common measures of ruggedness include the elevation range, or local relief (LR), and the standard deviation of elevation (s). LR is defined as the difference in elevation between the window maximum and minimum elevation values (Gallant and Wilson, 2000; Gallant et al., 2005; Liu, 2008). This measure is particularly sensitive to the elevation outliers and Gallant and Wilson (2000) caution that spatial patterns of LR can include abrupt changes where peaks fall in and out of the roving window. The elevation standard deviation is by comparison less sensitive to the extremes in elevation and is thought to better represent surface roughness properties (Evans, 1984; Klinkenberg, 1992). In the restricted case of a 3×3 window size, the terrain ruggedness index of Riley et al. (1999) is equivalent to s and is commonly calculated using GIS software.

Several terrain attributes are used to quantify the spatial pattern of topographic position, but the most common include elevation percentile (EP), difference from mean elevation ($DIFF$), and deviation from mean elevation (DEV). EP is the percentage of the cells within a roving window that are lower than the center pixel's elevation (Gallant and Wilson, 2000). It has a natural range from 0–100% and is relatively robust against elevation outliers. $DIFF$ is the difference between the window center's elevation and its mean elevation (Gallant and Wilson, 2000; Weiss, 2001). It has the same units as elevation and is either positive, indicating an elevated location, or negative, indicating a low-lying position. DEV is a unitless measure of topographic position and is calculated in the same way as $DIFF$ except that the elevation difference is normalized by s, such that:

$$\mathrm{DEV}\,(D) = \frac{z_0 - z_D}{s_D} \quad (1)$$

where D is the size of the window, z_0 is the elevation of the window center cell, and z_D is the window mean elevation. D is measured either in map units or grid cells. Since pixel-centered roving windows must have odd-numbered dimensions (3, 5, 7, etc.), it is more convenient to use the window half-size, r, where D

$= 2r + 1$. The series $r = 1, 2, 3,\ldots$ therefore describes the series of square pixel-centered windows, such that $r = 1$ denotes a 3×3 roving window, $r = 2$ denotes a 5×5 window, and so on.

While *DEV* is essentially the spatial pattern of local z-scores, this fact does not imply that the index can be used to determine the statistical probability of a particular value occurring (i.e. outlier detection) because elevation distributions are often non-Gaussian. Nonetheless, values of *DEV* do tend to lie well within the range -3.0 to 3.0. Unlike *DIFF*, *DEV* is a measure of relative topographic position that is scaled by the local ruggedness. This characteristic is particularly useful in applications involving heterogeneous landscapes (De Reu et al., 2013).

2.2. Integral images and spatial filtering

An integral image (I), also known as a summed area table, is a simple data transformation used to efficiently measure the sum of all values within rectangular sub-sets of a raster grid (Crow, 1984). A pixel value in I is the sum of the pixel values in the input image within the rectangular region defined by the pixel and an image corner, usually the upper left-hand corner, i.e. the image origin coordinate (0, 0) (Figure 1A). I is similar to a two-dimensional cumulative distribution function. After the integral image transform is applied, the sum of a rectangular neighborhood centered on a pixel is computed using three mathematical operations (Figure 1B) regardless of the neighborhood size. The mean value of any sub-region is then calculated by dividing the neighborhood total value by the number of pixels within the sub-region. An integral image based approach therefore enables the efficient calculation of many common image filtering operations using very large window sizes in a way that is impractical using traditional filtering methods.

Integral images make the calculation of *DIFF* trivial even when using very large window sizes. Importantly, a single integral image can be used to efficiently calculate the elevation residual not just for a single scale (window size) but rather for an entire range of scales. There is no need to recalculate I for each window size. It is this characteristic that enables an integral image based multi-scale approach to analyzing ruggedness and relative topographic position.

In addition to *DIFF*, it is also possible to calculate *DEV* using an integral image based approach. To do so requires the calculation of the first and second power integral images I and I^2. A second-power integral image is derived from squared input values. Given the sum and squared-sum values within a window, the standard deviation is estimated using one of the common single-pass algorithms. It is also possible to calculate skewness and kurtosis for large windows with this method, requiring I^3 and I^4 respectively, enabling a multi-scaled approach to the measurement of some of the terrain characterization methods proposed by Evans (1984) and later by Klinkenberg (1992).

The integral image approach can be extended to calculate other frequency dis-

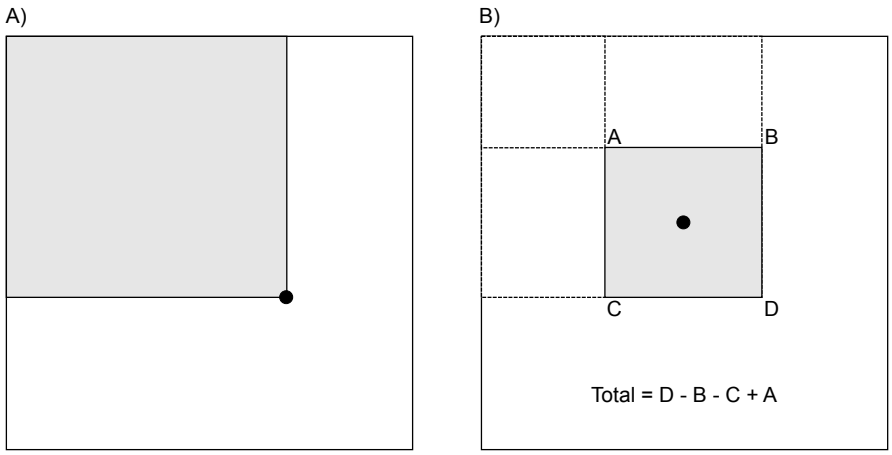

Figure 1: Integral image concept (adapted from Crow, 1984). A) The value of a pixel in an integral image is the sum of pixel values in the original image in the shaded area to the upper-left of the pixel. B) Sum values are calculated for rectangular sub-regions of an integral image using the addition and subtraction of the integral values of the four corners of the region.

tribution properties through use of integral histograms (Porikli, 2005). Rather than storing an individual sum value in each pixel, an integral histogram is a data structure in which each cell in the raster grid contains a histogram of values within the region defined by a pixel and the image origin corner. In this way, it is possible to describe the full frequency distribution of values contained within any arbitrary sub-region of an image. The integral histogram can be used to estimate summary statistics such as the median, interquartile range, and percentile. Thus, using this approach, it is possible to estimate *LR* and *EP* from a DEM for much larger window sizes than would be practical otherwise. However, since an integral histogram is essentially a three-dimensional image stack (rows $\times$ columns $\times$ histogram bins), or data cube, system memory constraints limit their practical application (Sizintsev et al., 2008). Furthermore, because calculations are based on the grouped data of histograms, the accuracy of *LR* and *EP* estimates derived using this technique are dependent on the binning strategy used.

3. Methods

3.1. Study area and topographic data

The study area spanned an extensive region of eastern Canada and the United States (40°N to 50°N and 7°W to 80°W). The site, consisting of three distinct

geological domains (Figure 2), was intentionally chosen to represent the heterogeneity of a diverse and complex landscape at the broadest spatial scales. Regional topographic elements are controlled by continental scale tectonic elements and fault-bounded basins (e.g. the Ottawa Valley). The northern region of the study area is underlain by the Canadian Shield and is part of the mesoproterozoic Grenville orogenic province. It is characterized by sedimentary, volcanic, granitoid gneisses and intrusive rocks (Davidson, 1998). The region is subdivided into a number of lithological and structural terrains commonly delimited by recessively eroded shear and fault zones, along with areas of intrusive plutonic rocks. These terrains can individually or as groupings coincide with distinct physiographic regions. For example the Grenvillian Adirondack physiographic region is composed of an anorthisite massive, metasedimentary rocks, and granitic intrusions.

The Appalachian tectonic front defines the northern edge of the Appalachian mountains and in Quebec occurs within the broad St. Lawrence River Valley, trending southward along the Great Valley segments of Lake Champlain and then westward south of the Adirondack Mountains along the Mohawk Valley. The Appalachians are characterized by a number of Lower Paleozoic tectonic zones and secondary belts of Middle Paleozoic rocks that have lithological, stratigraphic and thickness variations across the orogeny (Williams, 1995). Major physiographic elements of the orogenic belt are from south to north; in Pennsylvania the Appalachian Plateau, and Ridge and Valley; in New York the Adirondacks, and through New England and Quebec the Connecticut-Gaspe and Central Main troughs (Epstein, 1986; Hibbard et al., 2006).

The intervening area between these two major orogenic belts is the St. Lawrence Lowlands and extends from East–West along the St. Lawrence River into the Lake Ontario basin and north along the Ottawa Valley. Low altitude, subhorizontal, mildly deformed Paleozoic sandstone and carbonate rock are overlain by Quaternary mud and glacial sediment. The landscape of the eastern St. Lawrence Lowlands and the Champlain Valley are predominantly controlled by Champlain Sea glacimarine mud and subsequent fluvial incision. Lowland area to the west in the Lake Ontario basin is predominately drumlinized till (e.g. Peterborough and New York State drumlin fields) and stratified moraines (Oak Ridges Moraine and Valley Heads Moraine). Noteworthy in the St. Lawrence Valley are a series of nine small igneous intrusion of Cenozoic age know as the Montregian hills. The intrusions rise abruptly from the lowlands and northern Appalachians in an area extending eastward of Montreal (Roulleau and Stevenson, 2013).

Glacial sediment is generally thin and discontinuous across the Grenville and Appalachian terrains, with the exception of lower lying areas such as the Champlain, Mohawk and Hudson river valleys. The morphological signal of uplands is dominated by underlying differential bedrock erosion and structural control. Whereas in lowland areas surface morphology is predominantly a reflection of two components, including the paleoglacial landforms and proglacial to post

Figure 2: Study area DEM including parts of the Canadian Shield, Saint Lawrence Lowlands, and the northeastern Appalachian Mountains. Seven locations for which the *DEV* scale signatures are derived are marked and numbered.

glacial depositional environments (Champlain Sea, Lake Iroquois, Vermont and Champlain) and erosional processes including river incision (e.g. St. Lawrence).

Most of the study area is north of the southern extent of the Laurentide Ice sheet (Dyke et al., 2003). Southern parts of the study area in Pennsylvania are characterized by fluvial drainage signatures. This landscape signature is also present for a short distance north of the Laurentide ice sheet extent, notably in the Appalachian Plateau and Catskill Mountains.

Multi-scale topographic position analysis for the study area was based on 3-arcsecond Shuttle Radar Topography Mission (SRTM) version 4.1 seamless DEM data (Jarvis et al., 2008). SRTM data have a 90% absolute error of approximately 6.5 m over North America (Rodriguez et al., 2005). The data were retrieved from the CGIAR Consortium for Spatial Information public data portal as individual 5° × 5° tiles. The tiles were mosaicked and re-projected using nearest-neighbor resampling into the Universal Transverse Mercator (UTM zone 18N/WGS84) projection with an 82 m grid resolution. Void areas in the original SRTM data were filled by the data provider using a combination of interpolation techniques and auxiliary elevation data sources (Jarvis et al., 2008). The final DEM (Figure 2) was 13,692 × 10,413 rows by columns and was stored in a 544 MB single-precision floating-point data file.

3.2. Multi-scale calculation of elevation residuals

A set of three software tools for measuring *DEV*, each based on deriving integral images from an input DEM, were developed as plugins for the open-source geographical information system Whitebox Geospatial Analysis Tools v. 3.2 (Lindsay, 2014). Because *DEV* combines both *DIFF* and s in its calculation, the plugin tools are easily modified to output these additional topographic attributes. The plugin tools included:

1) A tool for measuring the high-resolution scale signatures of *DEV* for a specified set of point locations (i.e. single grid cells in the input DEM), called *Relative Topographic Position Scale Signature*,

2) A plugin tool for measuring the spatial pattern of *DEV* at the scale of the maximum absolute *DEV* value within a specified scale range ($DEV_{\max}$), called *Maximum Elevation Deviation*, and

3) A tool called *Create Multi-scale Topographic Position Image* for combining three $DEV_{\max}$ images to create a multi-scale topographic position color composite (MTPCC) image for the purpose of effective visualization and interpretation.

Each of the plugins can be called through graphical user interfaces, which are used to specify the various required input parameters. The plugin

tools are open-source licensed (GNU General Public License v. 3) and are distributed in a recent version of the Whitebox GAT software. The source code of the tools can be obtained from the Whitebox GAT project website (http://www.uoguelph.ca/~hydrogeo/Whitebox/). In addition to the Whitebox GAT plugins, and to further increase the end-user accessibility of the multi-scale topographic position analysis methods described in this paper, the tools were also replicated using the Go programming language as stand-alone applications that were not reliant on a specific GIS. These tools and their associated source code have also been made available through open-source licensing, and are also available through the Whitebox GAT website. Note that the algorithms described above are each serial and no efforts were made to parallelize the tools.

Integral images have previously been applied to image data types rather than DEM rasters. DEMs differ from images in that 1) they often contain elevations stored as floating-point numerical values (image data usually consists of integer data), 2) DEMs often have large value ranges (1000's or even 10,000's depending on the measurement units) compared with the typical image 8-bit (per color channel) range of $0-255$, and 3) DEM data frequently contain null values or a special *NoData* value. These first two characteristics are significant because they increase the likelihood of experiencing a numerical overflow error when calculating I and I^2 images from an input DEM. The need to avoid overflow errors was a primary development consideration. To reduce the potential for overflows, double-precision (64-bit) floating-point values were used to store the I and I^2 images in system memory. Also, shifting the elevation values in the input DEM by a constant factor does not affect the estimate of *DEV*. Therefore a constant value was subtracted from elevations before performing the I and I^2 transformations, further reducing the potential for overflow errors. The average of the DEM minimum and maximum elevations was used for the constant shift parameter.

NoData values in DEM data were handled by treating the pixel values as zeros, i.e. they did not influence sum values in I and I^2. However, *NoData* values in the input DEM meant an additional integral image was required to calculate the number of valid (non-*NoData*) grid cells within roving windows. Unlike the other two integral images, these data were stored using a 32-bit signed integer data type to reduce the memory requirements of the tools. Importantly, this allows for the processing of raster DEMs containing a maximum of approximately 4.3 billion grid cells, although available system memory can provide another constraint on the maximum DEM size. Note that no memory overflow errors were encountered during development and testing of the *DEV* tools, despite the large size of the study area DEM.

The use of integral images allows for very dense sampling of the scale signature of DEM elevation residuals. It is computationally feasible to calculate hundreds or even thousands of elevation residual rasters using this approach in order to fully resolve the scale signature of each grid cell in a DEM. However, doing so

would require storing a very large number of raster to disc, which may not be practical depending on DEM size. For example, resolving the scale signatures for the range $1 < r < 2600$ for each grid cell in the study area DEM would be over 1.4 TB of generated data. Therefore a method of summarizing the information contained within the scale signatures over scale ranges was required.

DEV rasters were calculated at a relatively dense scale interval but information was only stored about the largest magnitude, regardless of sign, *DEV* value ($DEV_{\max}$) and the scale at which it occurred ($r_{\max}$) for each grid cell. Thus,

$$r_{\max} = \arg \max \left(|\mathrm{DEV}\left(r_0\right)| \ldots |\mathrm{DEV}\left(r_N\right)| \right) \quad (2)$$

for the set of N roving window half-sizes from r_0 to r_N with a defined regular increment step value. $DEV_{\max}$ is therefore equivalent to $DEV(r_{\max})$. The mathematical operation arg max simply returns the index in a series that is coincident with the maximum series value. Notice that while $r_{\max}$ is calculated using absolute values of *DEV*, $DEV_{\max}$ retains the signed quantity of *DEV*. Importantly, this approach enables the estimation of an elevation residual value at the most deviated scale within tested scale ranges for each grid cell within the DEM. A $DEV_{\max}$ raster is essentially a composite dataset of the collection of *DEV* rasters within the tested scale range, where each cell is assigned the most deviated *DEV* value over the range.

4. Analysis

4.1. *DEV* scale signatures

The scale signature is a function that characterizes a measure of the topographic position of a location on Earth's surface relative to its surroundings across a range of spatial scales. In this sense, it is analogous to the spectral signature of remote sensing, which relates surface reflectance for varying wavelengths of electromagnetic energy, or the semivariogram of geostatistics, which relates the variance among point measurements offset by a range of lag distances. Figure 3 shows example scale signatures of *DEV* for the seven locations within the study area highlighted in Figure 2. The signatures are sampled with r ranging from 1 to 2500 grid cells (i.e. window sizes ranging from 7×7 to 5001×5001) using an increment step of one cell.

Although each grid cell in the DEM has a unique scale signature, the seven locations depicted in Figure 3 were selected to provide representative examples of observed signature trends. The following general characteristics were found to be common among most of the extracted scale signatures. First, signatures typically exhibited the greatest variability at the shortest range of spatial scales, often within the range $0 < r < 100$. Within this local scale range, signatures often possessed multiple peaks and troughs. Location 7 (Figure 3B), a site situated in a wide valley within the Ridge and Valley Province, is typical of the complexity of short-scale signatures. Secondly, while scale signatures typically

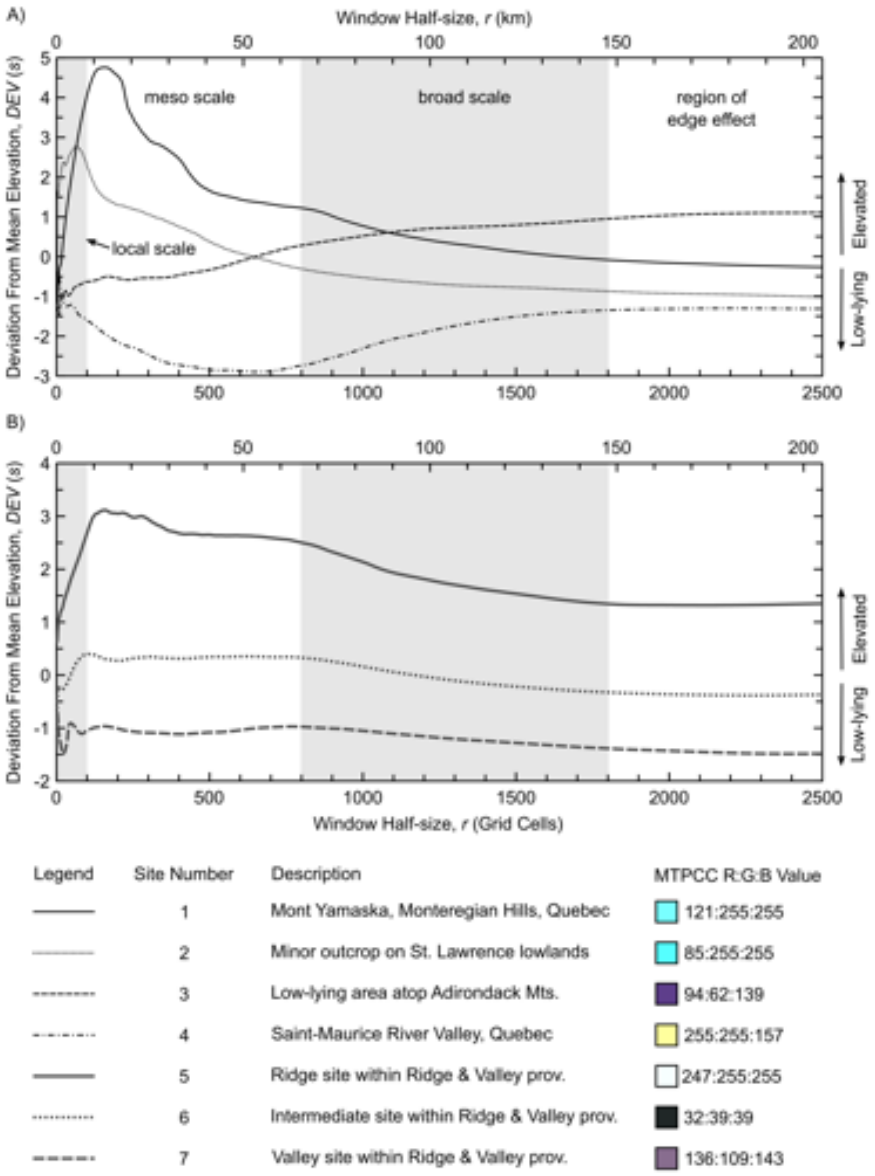

Figure 3: Example scale signatures of DEV for seven locations within the study area, including A) four sites dispersed throughout the study region, and B) three nearby sites within the Ridge and Valley Province. Three ranges of spatial scales (local, meso, and broad), which were used to derive $DEV_{\max}$ rasters, are labeled and shaded. The red:green:blue color of the corresponding pixel in the MTPCC image (Figure 5) is also provided.

had fewer inflections within the mid-range of scales ($100 < r < 800$), signatures did often exhibit large peaks or troughs in this range. Location 1 (Figure 3A), situated atop Mont Yamaska within the Monteregian Hills, is an example of a site that possessed a large peak in this region. Third, variations in scale signatures within the broad range of approximately $800 < r < 1800$ were more subdued with lower peaks/troughs or, more commonly, monotonic variation in DEV with increasing spatial scale. While shallow peaks and troughs were observed in some locations within this broad scale range, each of the seven example signatures exhibited the more common scenario of monotonically increasing or decreasing DEV at broader spatial scales (Figure 3). Lastly, at scales greater than approximately $r = 1800$, all scale signatures became level with very little further variation. While the boundaries between the scale ranges described above are approximate, and are likely unique to the study area and data used in this analysis, these general observations appear to be ubiquitous.

Finely sampled scale signatures, such as the examples in Figure 3, enable the detailed analysis of the relative topographic position of sites across a range of spatial scales. For example, the scale signatures of Locations 1 and 2 (Figure 3A) are similarly shaped; however, the peaks in the two signatures show that Location 1 is most prominently deviated at a longer spatial scale of 12.7 km (window half-size) compared to the most prominently elevated scale of 5.5 km for Location 2. The height of the Location 1 peak is also greater, indicating that Mont Yamaska is more deviated within the context of its local surroundings. Mont Yamaska remains relatively elevated at longer spatial scales until it occupies an average topographic position at scales larger than about 136 km. Location 2, also situated on the St. Lawrence Lowlands, occupies a relatively low-lying position in the landscape at similarly broad scales. The scale signature of Location 3, situated within the Adirondack Mountains, is a mirror opposite of Location 2. Its signature exhibits a relatively low-lying topographic position at shorter scale ranges and a more elevated position in the broader landscape at scales larger than 50 km. In contrast, Location 4, positioned along the Saint-Maurice River Valley in Quebec Canada, remains low-lying across all tested spatial scales, with its most deviated position coinciding with a DEV minima point in a wide trough in the signature at approximately 52.5 km.

Figure 3B shows the scale signatures of three nearby sites situated within the Ridge and Valley Province of Pennsylvania, USA. Location 5 is situated atop a ridge location; Location 6 is an intermediate site; and Location 7 is positioned along a wide valley floor. Although at local and meso-scales the signatures exhibit complexities indicative of the unique positioning of each site, at scales longer than 100 km, the three signatures are parallel. The three sites are so close to one another, that at these scales, the roving window centered on each of the sites overlap to the extent that they have nearly identical means and standard deviations. It is this property that results in parallel scale signatures for closely located sites at broad scales.

One of the observations of all tested scale signatures was the leveling of the DEV-

scale relation at a near constant value at the broadest spatial scales. Why is this property of scale signatures so prevalent? Once window sizes become large, the mean and standard deviation of the window become good estimates for the overall DEM mean and standard deviation. Thus, the convergence value for a location is equal to the difference in elevation between the site and the mean elevation of the DEM, normalized by the DEM's standard deviation, i.e. the DEM-wide z-score transformation. Therefore, at these broadest scales, the estimate of DEV is equivalent to a standardized shift of the DEM's datum from sea level to the DEM mean elevation.

As the window size approaches the dimensions of the raster, they will overlap with increasingly larger portions of the available elevation data. However, larger-sized windows will also have extensive areas beyond the edge of the DEM where elevation data are not available to the analysis (windows are necessarily truncated at grid edges). As such, the convergence of scale signatures to a stable value is an edge effect associated with larger window sizes and represents an upper limit on the scale from which useful information can be extracted from the DEM. This upper limit could be determined by identifying the scale at which a certain percentage of grid cells have DEV values that are different from the corresponding z-score transform of the cell's elevation by a specified threshold. Alternatively, one could determine the upper scale limit as the largest scale at which correlation between DEV and the DEM drop below a specified threshold or significance value.

If additional data were available for the region beyond the edge of the grid, it is likely that the scale signature would continue to relay useful information about the topographic character of the surface at broader scales. Coastlines also present a type of edge effect for these analyses, and taken to the extreme, the continent boundaries provide a practical upper scale limit, unless bathymetric data are incorporated into the analysis. As with all topographic attributes that are impacted by edge effects, this problem is best handled by analyzing a subregion buffered by elevation data on the margins where it is practical to do so.

4.2. DEV_{max} rasters

Based on the scale signature data (Figure 3), the spatial pattern of $DEV_{\max}$ was derived for the study area DEM for three widely spanning ranges, referred to as the local, meso-, and broad scales (Figure 4). The scale ranges corresponded to r ranges, measured in grid cells, of 3–99 (0.2–8.1 km), 100-795 (8.2–65.2 km), and 800–1800 (65.6–147.6 km) with sampling densities (i.e. the interval in r between consecutive DEV images in the range) of 1 cell (0.09 km), 5 cells (0.43 km), and 10 cells (0.85 km), respectively. Based on these ranges and sampling densities, the three output DEV_{max} rasters (Figure 4) were derived from 338 individual DEV rasters (which only existed temporarily in system memory) with varying roving window dimensions ranging from 7×7 to 3601×3601 grid cells.

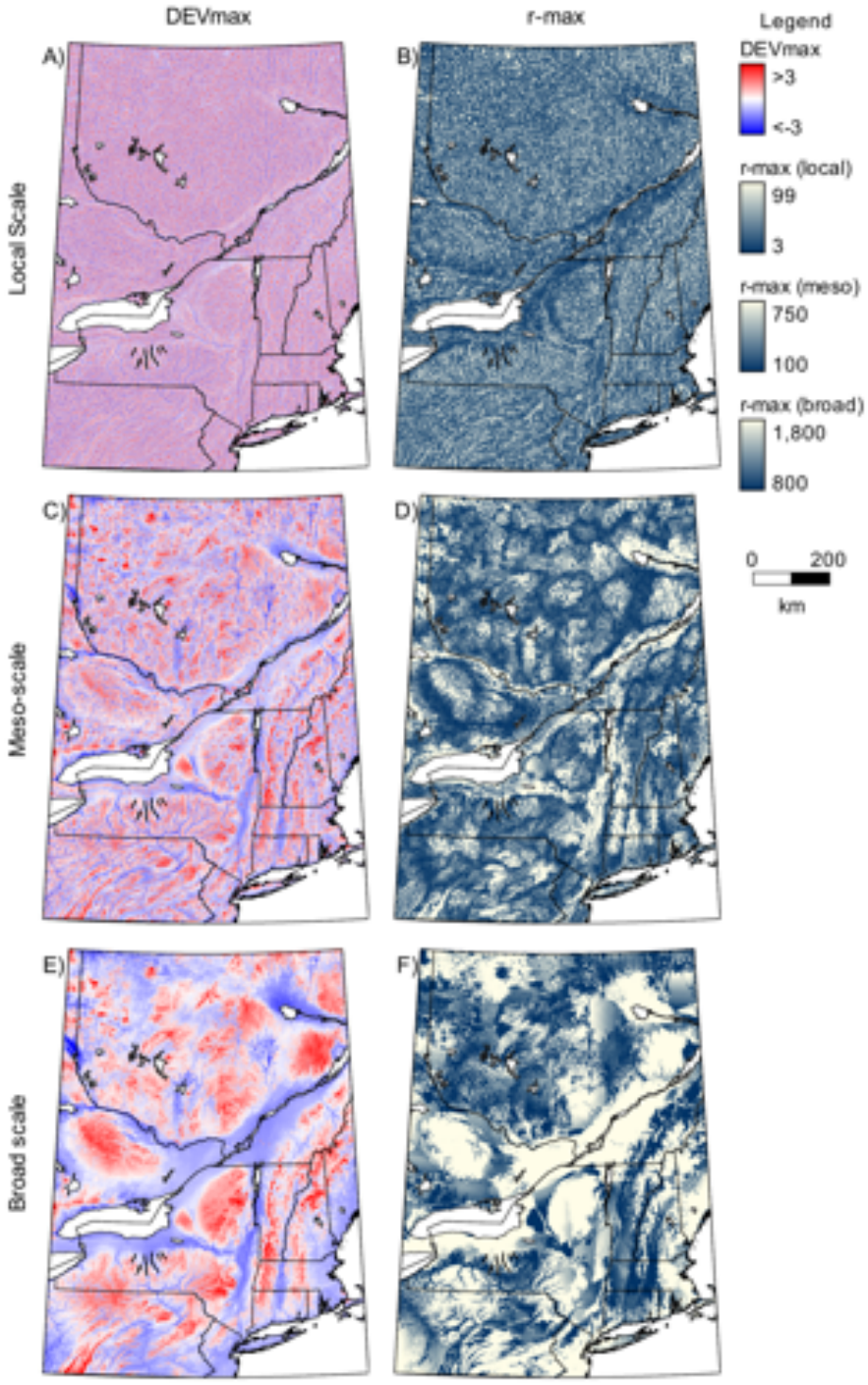

Figure 4: Spatial patterns of $DEV_{\max}$ at the local (A), meso- (C), and broad (E) scales and $r_{\max}$ at the local (B), meso- (D), and broad (F) scales, with spatial scales defined as in Figure 3.

The local-scale range $DEV_{\max}$ raster (Figure 4A) was created in 8.55 minutes on a computer with a 3.0 GHz processor and 64 GB of 1866 MHz DDR3 memory. The meso-scale (Figure 4C) and broad scale (Figure 4E) $DEV_{\max}$ rasters were created in 11.15 minutes and 8.85 minutes, respectively. The time needed to compute a single DEV raster with one roving window size for the study DEM was approximately 5.5 seconds regardless of the window size. It is apparent from these findings that the integral image based approach to calculating elevation residual rasters allowed for efficient processing even using roving window sizes much larger than the windows that have been previously used for elevation residual analysis in the published literature.

It was not possible to use the traditional roving window approach to calculate the three $DEV_{\max}$ rasters in Figure 4 to provide a comparison, due to computational inefficiency. Experiments were carried out calculating DEV on the test DEM using roving windows of varying sizes up to $r = 50$, which required 13,648 seconds to process. Based on this work, the DEV raster with the largest search window ($r = 1800$) used in this study would take approximately 122 days to calculate, compared with the 5.5 seconds required by the integral image approach used in this work. It is estimated that calculating the same 338 DEV rasters that were used to create the local, meso-, and broad scale range $DEV_{\max}$ rasters would take approximately 23.3 years to process. By comparison, the integral image approach required a total of 28.5 minutes to compute these same three rasters.

The $DEV_{\max}$ and r_{max} rasters (Figure 4) both provide information about the topographic character of the landscape of the study area across a wide range of spatial scales. $DEV_{\max}$, as a multi-scale elevation residual topographic attribute, summarized topographic position information across a finely resolved range of spatial scales in a manner where each pixel could be represented by its maximally deviate position. This approach is an improvement on what would be achieved if a single DEV raster at an ad-hoc scale were used to summarize topographic variability across a wide range of spatial scales. The most deviated position of a scale signature over a range will either coincide with the maxima/minima of a peak/trough or, in the case of monotonically varying signatures, with one boundary of the scale range. Often it is the peaks and troughs of the signature that are of greatest interest. The maxima and minima of peaks and troughs in a scale signature represent key scales at which a location occupies a strongly deviated topographic position relative to its surroundings and are usually associated with scales at which the site is most responsive to features within the landscape. For example, the maxima in the Location 5 signature (Figure 3B) at a window half-size of 13.1 km indicates that the ridge, atop which the site is located, is most well defined at this spatial scale. It is possible to use the data within $r_{\max}$ rasters to identify which grid cells have $DEV_{\max}$ values associated with signature peaks or troughs, as opposed to monotonically varying functions over the tested scale ranges. Doing so simply involves identify which grid cells have $r_{\max}$ values that are greater than the lower scale boundary and are less than the upper boundary of the tested range.

4.3. The multi-scale topographic position color composite

A multi-scale topographic position color composite (MTPCC) image was created to facilitate the visualization and interpretation of the multi-scale information contained within the three $DEV_{\max}$ rasters (Figure 5). Each pixel in the MTPCC image presents information about the topographic position of the pixel location at each of the three scale ranges in the form of a single 24-bit Red-Green-Blue (RGB) color. Table 1 presents a key for interpreting the information contained within the MTPCC image. The interpretation key is only provided as an aid, indicating what various exemplar colors mean with respect to the three spatial scale ranges. The key provides exemplar color combinations that represent extreme conditions where one or two scales are highly deviated (either high or low in the landscape) while the location occupies an average position in the remaining scales. For example, the color blue occurs where a site is highly deviated at the local scale but average in position at the meso- and broad scales. In reality, very few pixels in an MTPCC image are likely to be pure blue (RGB 0:0:255) but if there are blue-tinted pixels, it is apparent that the site is more strongly deviated at the local scale than either of the broader scales. A darker blue colored pixel (e.g. RGB 32:32:128) would indicate the site is not very deviated at any scale but more so at the local than any other. A light blue color (e.g. RGB 128:128:255) indicates the site is moderately deviated across all scales and more so at the local than either of the others. Similarly, while magenta (RGB 255:0:255) may not occur in Figure 5, there are regions of purple and pink colored pixels that follow the general pattern of being more strongly deviated at both the local and broad scales while being average in position at the meso-scale.

The MTPCC image was created by combining the $DEV_{\max}$ rasters of the local-, meso-, and broad-scale ranges into the respective blue, green, and red channels of a 24-bit color image. The three $DEV_{\max}$ rasters were first processed to linearly rescale their absolute grid cell values within the range 0-2.58 to the output 8-bit range of 0-255. Grid cells occupying an average landscape position within a particular range were therefore assigned the lowest values after rescaling. Highly deviated locations (i.e. exceptionally elevated or depressed sites) with input pixel values greater than the 2.58 cutoff value were assigned an output value of 255. The cutoff value of 2.58 was selected because the ± 2.58 standard deviation from the mean of a Gaussian distribution includes nearly 99% of the samples. Altering the cutoff value has the effect of modifying the overall brightness of the image.

The MTPCC image (Figure 5) was found to be an effective means for visualizing the scale-variant topographic character of a landscape. Visual inspection showed that the density of topographic information within these images is very high, even compared with other common means of visualizing terrain data such as a DEM rendered with analytical hillshading (Figure 6). A MTPCC image summarizes the relative topographic position of sites across three defined ranges of spatial scales simultaneously. For example, note how the Monteregian Hills, a

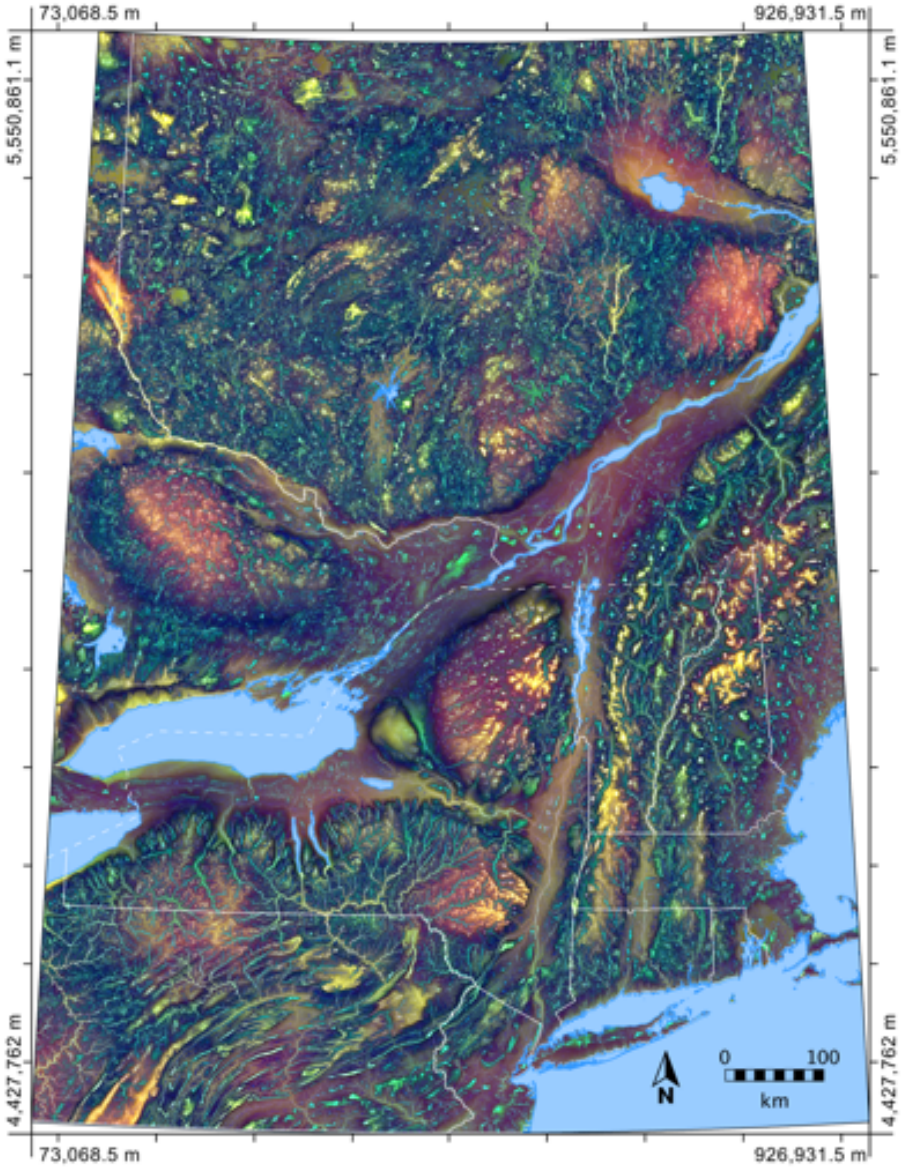

Figure 5: A multi-scale topographic position color composite (MTPCC) image created by combining $DEV_{\max}$ rasters from the three scale ranges into the red-green-blue channels of a 24-bit color image.

linear chain of rounded hills in the St. Lawrence River Valley (bottom of Figure 6C), are brightly green-cyan colored. This indicates their prevalent topographic position across the local and meso-scales and corresponds to the peak in the Location 1 signature within the meso-scale range in Figure 3A. Also observe how the large fissures of the Laurentian Uplands (Figure 6C) and the deeply incised river valleys of the Catskill Mountains (Figure 6A) are most responsive at a smaller spatial scale (local to meso) than the upland areas that they occupy (i.e. red-yellow coloring indicates a strongly deviated position at the meso- to broad scales).

Table 1: A key for interpreting MTPCC images.

Color	**Interpretation**
Blue-tinted	Strongly deviated (either elevated or low-lying) local-scale position; average landscape position at the two larger scales.
Green-tinted	Strongly deviated meso-scale position; average landscape position at both the local and broad-scale range.
Red-tinted	Strongly deviated broad-scale position; average landscape position at both of the shorter scales.
Cyan	Strongly deviated position at both the local and meso-scale ranges; average landscape position in the broad-scale range.
Yellow	Strongly deviated position at the meso- and broad-scale ranges; average landscape position in the local-scale range.
Magenta	Strongly deviated position at the local and broad-scale ranges; average landscape position in the meso-scale range.
Dark grey and black	Average landscape position across a wide range of spatial scales.
Light grey and White	Deviated landscape position (elevated or low-lying or both, i.e. elevated at one scale and low-lying at another) across a wide range of spatial scales.

This localized color contrast between landscape features (e.g. ridges, incised river valleys, and hills) and the broader context in which the features are superimposed is one of the reasons why the MTPCC image is so effective at visualizing terrain. In addition to this color contrast, the MTPCC image benefits from the fact that prominent landscape features are outlined by thin dark-colored lines, which serve to emphasize salient features. This is most obvious when viewed in detail but is exemplified by the dark line separating the eastern edge of the

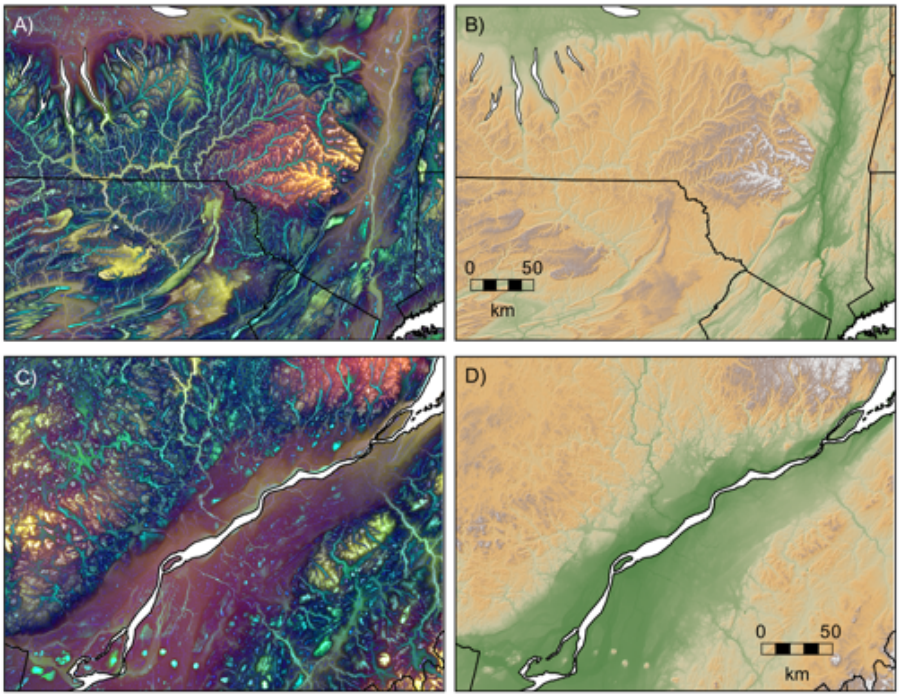

Figure 6: Detailed comparisons of the MTPCC image (A and C) and analytically hillshaded DEMs (B and D) of a section of the Catskill Mountains region (A and B) and the St. Lawrence Lowlands/Laurentian Uplands region (C and D).

Catskill Mountains and the Hudson River Valley (Figure 6A). These lines are coincident with sites of average relative topographic position across wide ranges of spatial scales. The Location 6 signature (Figure 3B) of the intermediate site within the Ridge and Valley Province is an example of one such site possessing an average topographic position across all three of the tested scale ranges. In fact, when examined closely, many of the ridges within this region are very well highlighted by these dark outlines, which serve to define their boundaries (Figure 6A).

The MTPCC image is the multi-scale interpretation of relative topographic position in the same way that a false-color satellite image provides a multi-spectral interpretation of surface reflectance. Similar to how experimentation with various combinations of satellite image bands is needed to create an effective composite visualization, some experimentation with the positioning and boundaries between scale ranges in the input $DEV_{\max}$ rasters is required to create an effective MTPCC image from a DEM. Also, some practice with the image is required to train the eye to recognize colors as the summation of relative topographic position across three scale ranges, rather than, for example, as the raw elevation observed in a DEM.

5. Discussion

Given the high computational cost associated with filter-based neighborhood analysis (Deng and Wilson, 2008; Grohmann and Riccomini, 2009), much of the previous research has relied on altering DEM grid resolution using either aggregation or resampling methods (e.g. Gallant and Dowling, 2003; Deng and Wilson, 2008) or on hierarchical object-based DEM segmentation (e.g. Drăgut and Eisank, 2011; Drăgut et al., 2011) to study the scale varying character of terrain attributes. Both of these approaches have limitations. Drăgut et al. (2011) demonstrate how degrading grid resolution has the effect of smoothing the DEM and reducing local variance, which is counter to the purpose of evaluating the scale-dependency of terrain ruggedness and relative position. Object-based approaches, like all image segmentation methods, require careful parameterization, which can be challenging. The integral image based method used in this study has allowed for highly detailed multi-scale evaluation of relative topographic position at vast spatial extents, without resorting to data degradation. This approach has allowed for the study of topography at widely varying scale ranges from scales associated with individual landforms to the scale of entire mountain ranges. These data are only made possible by the extremely computationally efficient and window-size independent manner in which DEV is calculated using an integral image based method.

Measures of terrain ruggedness and relative topographic position have been widely applied to automated landform classification and characterization of terrain heterogeneity (Riley et al. 1999; Tagil and Jenness, 2008; De Reu et al., 2013). The combined information contained within $DEV_{\max}$ and $r_{\max}$ rasters

will enhance automated landform classifications because it enables multi-scale data inclusion compared with the results obtained by inclusion of a DEV raster derived from a single scale. De Reu et al. (2013) recently demonstrated how the application of DEV data sampled at multiple scales using varying neighborhood sizes could enhance landform classifications. $DEV_{\max}$ has the benefit of representing relative topographic position at critical scales for each individual grid cell with respect to the shape of their unique scale signatures compared with the use of a relatively sparse sampling of DEV rasters across a range of scales with arbitrary intervals in neighborhood sizes.

The MTPCC image, or the $DEV_{\max}$ rasters from which they are derived, could serve as the input for a cluster analysis to identify groups of pixels with similar scale signatures. Close inspection reveals that much of the information contained within the MTPCC image is in the form of localized patterns of texture, which define areas of interest with respect to their topographic setting. Thus, texture-based classification methods (e.g. Chica-Olmo and Abarca-Hernandez, 2000) may also be of interest in further analyzing these data. The potential for calculating $DEV_{\max}$ rasters using rectangular-shaped windows also provides the opportunity to examine anisotropy (i.e. directional dependency) in the spatial patterns of relative topographic position, adding a further dimension to their interpretation. Ultimately these data provide a rich basis for performing multi-scale relative topographic position and ruggedness analyses using DEMs at spatial scales that are relevant for evaluating the structure of heterogeneous landscapes.

6. Conclusions

This study was a multi-scale topographic position analysis performed on a large DEM of an extensive region in eastern North America. The analysis was based on the common scale-dependent elevation residual attribute deviation from mean elevation. Three open-source software tools were created to allow for the derivation of the terrain attribute both at large spatial scales and with a high sampling density of scale ranges. The following conclusions can be drawn from the finding of this study:

1. An integral image approach allows for the efficient computation of DEV, and its composite terrain attributes, difference from mean elevation ($DIFF$), and standard deviation in elevation (s). This method provides the opportunity to study the multi-scaled properties of relative topographic position and landscape ruggedness at resolutions and spatial scales not previously possible using a roving window approach without resorting to degrading data resolution. This can potentially reveal valuable insight into landscape structure across spatial scales and may be useful for applications of topographic position and ruggedness, namely automated landform classification as well as soil, vegetation, and habitat mapping.

2. As a multi-scale topographic attribute, $DEV_{\max}$ provides a valuable means of summarizing topographic position information for each pixel in a DEM at key spatial scales within a wider range of scales. This has advantages over the ad-hoc means by which previous work has sampled the scaling properties of elevation residual parameters through the sparse selection of roving window dimensions. In addition, the spatial pattern of $r_{\max}$, i.e. the scale associated with maximal topographic position deviation, can also provide useful information for the common applications of these data.

3. The novel development of the MTPCC image, derived by combining three $DEV_{\max}$ rasters into a single color composite image, provides a convenient means of interpreting the multi-scale properties of locations within the landscape. The information density contained within these images is on par with or exceeding that of other commonly applied terrain visualization methods such as analytical hillshading.

Future work will focus on developing and refining integral-histogram based approaches to the multi-scale estimation of terrain attributes that require characterization of the full frequency distribution of elevations within local neighborhoods. While currently limited by the constraints of handling massive data volumes, these approaches offer the promise of new avenues for DEM-based landform characterization using histogram-search operations.

Acknowledgements

This work was partially funded through a grant provided by the Natural Sciences and Engineering Research Council of Canada (NSERC; grant number 400317). This is ESS Contribution number 20150085.

References

Böhner, J., Antonic, O., 2009. Land surface parameters specific to topoclimatology, in: Hengl, T., Reuter, H. (Eds.), Geomorphometry: Concepts, Software, Applications, Developments in Soil Science Series. Elsevier, Amsterdam, pp. 195–226.

Chang, K., Tsai, B., 1991. The effect of DEM resolution on slope and aspect mapping. Cartogr. Geogr. Inf. Syst. 18, 69–77.

Chica-Olmo, M., Abarca-Hernandez, F.. 2000. Computing geostatistical image texture for remotely sensed data classification. *Comp. & Geosci* 26(4), 373–383.

Crow, F.C., 1984. Summed-area tables for texture mapping. Comput. Graph. 18, 207–212.

Davidson, A., 1998. An overview of Grenville Province geology, Canadian shield. Geol. Precambrian Super. Grenv. Prov. Precambrian Foss. N. Am. Ed. SB Lucas MR St-Onge Geol. Surv. Can. Geol. Can. 7, 205–270.

De Reu, J., Bourgeois, J., Bats, M., Zwetvaegher, A., Gelorini, V., Smedt, P.D., Chu, W., Antrop, M., De Maeyer, P., Finke, P., van Meirvenne, M., Verniers, J., Crombe, P., 2013. Application of the topographic position index to heterogeneous landscapes. Geomorphology 186, 39–49. doi:10.1016/j.geomorph.2012.12.015

Deng, Y., Wilson, J.P., 2008. Multi-scale and multi-criteria mapping of mountain peaks as fuzzy entities. Int. J. Geogr. Inf. Sci. 22, 205–218. doi:10.1080/13658810701405623

Deng, Y., Wilson, J.P., Bauer, O., 2007. DEM resolution dependencies of terrain attributes across a landscape. Int. J. Geogr. Inf. Sci. 21, 187–213. doi:10.1080/13658810600894364

Drăgut, L., Eisank, C., 2011. Object representations at multiple scales from digital elevation models. Geomorphology 129, 183–189. doi:10.1016/j.geomorph.2011.03.003

Drăgut, L., Eisank, C., Strasser, T., 2011. Local variance for multi-scale analysis in geomorphometry. Geomorphology 130, 162–172. doi:10.1016/j.geomorph.2011.03.011

Dyke, A.S., Moore, A., Robertson, L., 2003. Deglaciation of North America. Geological Survey of Canada Ottawa, ON.

Epstein, J.B., 1986. The Valley and Ridge Province of eastern Pennsylvania—stratigraphic and sedimentologic contributions and problems. Geol. J. 21, 283–306.

Evans, I., 1984. Correlation structures and factor analysis in the investigation of data dimensionality: statistical properties of the Wessex land surface, England, in: International Symposium on Spatial Data Handling, Zurich. pp. 98–116.

Gallant, A.L., Brown, D.D., Hoffer, R.M., 2005. Automated mapping of Hammond's landforms. Geosci. Remote Sens. Lett. IEEE 2, 384–388.

Gallant, J.C., Dowling, T.I., 2003. A multiresolution index of valley bottom flatness for mapping depositional areas. Water Resour. Res. 39, 1347. doi:10.1029/2002WR001426

Gallant, J.C., Wilson, J.P., 2000. Primary topographic attributes, in: Wilson, J.P., Gallant, J.C. (Eds.), Terrain Analysis: Principles and Applications. John Wiley & Sons Inc., New York, pp. 51–85.

Goodchild, M.F., 2011. Scale in GIS: An overview. Geomorphology 130, 5–9. doi:10.1016/j.geomorph.2010.10.004

Grohmann, C.H., Riccomini, C., 2009. Comparison of roving-window and search-window techniques for characterising landscape morphometry. Comput. Geosci. 35, 2164–2169. doi:10.1016/j.cageo.2008.12.014

Hibbard, J., van Staal, C.R., Rankin, D., Williams, H., 2006. Lithotectonic Map of the Appalachian Orogen: Canada-United States of America. *Geological Survey of Canada, "A" Series Map*, issue 2096A.

Huggett, R., Cheesman, J., 2002. Topography and the Environment. Pearson Education Lt., Harlow.

Jarvis, A., Reuter, H.I., Nelson, A., Guevara, E., 2008. Hole-filled seamless SRTM data V4. Int. Cent. Trop. Agric. CIAT.

Jenness, J.S., 2004. Calculating landscape surface area from digital elevation models. Wildl. Soc. Bull. 32, 829–839.

Klinkenberg, B., 1992. Fractals and morphometric measures: is there a relationship? Geomorphology 5, 5–20.

Lindsay, J.B., 2014. The Whitebox Geospatial Analysis Tools project and open-access GIS. Presented at the GIS Research UK 22nd Annual Conference, Glasgow, UK.

Lindsay, J.B., Rothwell, J.J., 2008. Modelling channelling and deflection of wind by topography, in: Zhou, Q., Lees, B., Tang, G. (Eds.), Advances in Digital Terrain Analysis. Springer, Berlin, Heidelberg, pp. 383–405.

Liu, A., 2008. DEM-based analysis of local relief, in: Zhou, Q., Lees, B., Tang, G. (Eds.), Advances in Digital Terrain Analysis. Springer, pp. 177–192.

Pike, R.J., 2000. Geomorphometry—diversity in quantitative surface analysis. Prog. Phys. Geogr. 24, 1–20. doi:10.1177/030913330002400101

Pike, R.J., Evans, I.S., Hengl, T., 2008. Chapter 1 Geomorphometry: A brief guide, in: Hengl, T., Reuter, H. (Eds.), Geomorphometry: Concepts, Software, Applications, Developments in Soil Science Series. Elsevier, pp. 1–28.

Porikli, F., 2005. Integral histogram: a fast way to extract histograms in Cartesian spaces, in: Computer Vision and Pattern Recognition. Presented at the IEEE Computer Society Conference On CVPR 2005, San Diego, CA, pp. 829 – 836. doi:10.1109/CVPR.2005.188

Riley, S.J., DeGloria, S.D., Elliot, R., 1999. A terrain ruggedness index that quantifies topographic heterogeneity. Intermt. J. Sci. 5, 23–27.

Rodriguez, E., Morris, C., Belz, J., Chapin, E., Martin, J., Daffer, W., Hensley, S., 2005. An assessment of the SRTM topographic products. Jet Propulsion Laboratory, Pasadena, California.

Roulleau, E., Stevenson, R., 2013. Geochemical and isotopic (Nd–Sr–Hf–Pb) evidence for a lithospheric mantle source in the formation of the alkaline Monteregian Province (Quebec). Can. J. Earth Sci. 50, 650–666.

Sizintsev, M., Derpanis, K.G., Hogue, A., 2008. Histogram-based search: A comparative study, in: Computer Vision and Pattern Recognition. Presented at the IEEE Conference on CVPR 2008, Anchorage, AK, pp. 1–8. doi:10.1109/CVPR.2008.4587654

Tagil, S., Jenness, J., 2008. GIS-based automated landform classification and topographic, landcover and geologic attributes of landforms around the Yazoren Polje, Turkey. J. Appl. Sci. 8, 910–921.

Viola, P., Jones, M., 2001. Rapid object detection using a boosted cascade of simple features, in: Computer Vision and Pattern Recognition, 2001. CVPR 2001. Proceedings of the 2001 IEEE Computer Society Conference on. IEEE, pp. I–511.

Weiss, A., 2001. Topographic position and landforms analysis, in: Poster Presentation, ESRI User Conference, San Diego, CA. p. 200.

Williams, H., 1995. Temporal and spatial divisions, in: Williams, H. (Ed.), Geology of the Appalachian-Caledonian Orogen in Canada and Greenland. Geological Survey of Canada, Geology of Canada, pp. 21–44.

Wood, J., 1996. The geomorphological characterisation of digital elevation models. Unpublished Ph.D. dissertation, University of Leicester.

Yokoyama, R., Shirasawa, M., Pike, R.J., 2002. Visualizing topography by openness: a new application of image processing to digital elevation models. Photogramm. Eng. Remote Sens. 68, 257–266.